Spray in cross–flow: comparison of experimental and numerical approach

Ondrej Cejpek[1*], *Milan* Maly[1], *Miloslav* Bělka[1], *Jaroslav* Slama[2], *Ondrej* Hajek[1], *Frantisek* Prinz[1], and *Jan* Jedelský[1]

[1]Energy Institute, Faculty of Mechanical Engineering, Brno University of Technology, Technická 2896/2, 616 69 Brno, Czech Republic
[2]Provyko s.r.o., Vinařská 558/3a, Pisárky, 603 00 Brno, Czech Republic

Abstract. The spray behaviour and droplet trajectories in realistic conditions are of crucial importance in many industrial, agricultural and chemical applications. Droplet characteristics and spray trajectory in chemical applications (e. g. flue gas scrubbing, CO_2 capture in spray column) determine the amount of mass involved in the gas scrubbing process, mass trapped by the flow or attached to the walls. Knowledge of the droplet behaviour can improve a nozzle design and scaling, increase the process efficiency, minimize the process liquid and blow away the fraction. In this study, experiments with pressure swirl nozzle in cross–flow of air were performed at one nozzle injection pressure (0.5 MPa) and several cross–flow velocities (8, 16, 32 m/s). The results on droplet trajectories are compared with numerical results obtained by ANSYS Fluent. Two Lagrange approaches for spray modelling were used. Injection of droplet groups and Linearized Instability Sheet Atomization (LISA) model incorporated within ANSYS Fluent were used to represent the spray. The CFD results of spray penetration and droplet trajectories are compared with experimental data. A simple analytical model is able to well predict trajectories of large droplets, but fails to predict trajectories of small droplets. The LISA model yields a better accuracy for spray in cross-flow prediction.

1 Introduction

Pressure swirl atomizers are used in many industrial, chemical and agricultural applications. Cross-flow air simulates the conditions in combustion chambers, chemical processes dealing with gas scrubbing, agricultural spraying and many other realistic applications. Pressure-swirl atomizers are designed to produce a rapid break-down of liquid in a two-phase droplet flow. They are used to increase the specific surface area of the fuel and thereby achieving a high rate of mixing and evaporation. In most combustion systems, a reduction in mean drop size leads to higher volumetric heat release rate, easier ignition, a wide burning range and lower exhaust concentrations of the pollutant emissions [1]. In the gas scrubbing application, the increase in the interfacial area is also beneficial. The knowledge of spray behaviour and droplet trajectory is also crucial in order to determine and reduce the blown-away fraction.

This study combined the experimental and numerical approach to investigate the pressure swirl atomizer in the cross-flow condition. However, the experiments are usually time consuming and, in some cases, unrealizable. These drawbacks can be off-set by numerical modelling; this can be deployed beneficially to determine the spray characteristics in realistic conditions. Different numerical simulations are compared in this study.

Amedorme et al. [2] modelled the pressure-swirl atomizer in still ambient conditions. The Eulerian modelling of two-phase flow was employed in STAR-CD. Both internal and external flows were solved. Deshpande et al. [3] performed a computational analysis of hollow cone liquid injection into cross-flow. Lagrangian-Eulerian point parcel treatment of the spray was used in OpenFOAM. The authors classified the spray into the near and far field spray region, characterized by the drag force. The penetration of spray cone by the cross-flow was observed for high cross-flow velocities. Zhang et al. [4] numerically investigated the flow field structure of hollow cone spray injected into cross-flow. The Scale-Adaptive Simulation was employed to predict the turbulent flow. The atomization was modelled by Linear instability analysis and Taylor analogy breakup theory. Many different scaled vortices were identified around the hollow cone. Models for heat and mass transfer were also added to the sprays in cross-flow. Sun et al. [5] compared different models for heat and mass transfer for a spray injected to the cross-flow. Different corelations yield very different results on droplet evaporation. Dikshit et al. [6] simulated the pressure atomizer for small scale gas turbines applications. The study was mainly devoted to understanding of secondary droplet breakup.

Many different simulations of pressure-swirl atomizers and sprays with various physical models were performed. However, a simple and reliable model of

* Corresponding author: Ondrej.Cejpek@vutbr.cz

spray behaviour for the rapid prediction of droplet trajectories has not been developed and validated yet.

2 Experimental setup

Tests were performed at Spray research laboratory, Brno University of Technology.

2.1 Wind tunnel

A specially designed wind tunnel in blow down arrangement was used to simulate the flow condition. The flow parameters were probed using Laser Doppler anemometry prior to the measurement. The cross-flow velocity (v) and turbulent intensity (Tu) are outlined in Figure 1. Profiles in horizontal plane are presented. The vertical v and Tu profiles are symmetrical.

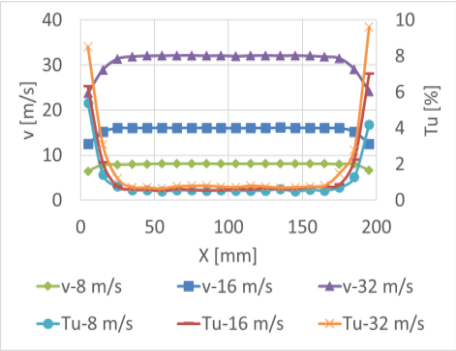

Fig. 1. Profiles of velocity and turbulent intensity in the wind tunnel test section

2.2 PDA measurement setup

Fiber based PDA system (Dantec Dynamics A/S Skovlunde, Denmark) was used to determine the droplet velocity and diameter. Three planes at axial distance Z = 10 mm, 15 mm and 20 mm from the nozzle tip were measured. At least 30 000 samples were acquired in each measurement position or for 10 s measurement duration. The Dantec BSA software 5.2 was used to control the measurement. PDA measurement setup is outlined in Figure 2. Two velocity components along with droplet size were measured in a coincidence mode. The laser output was set to 300 mW. Lenses with 500 mm focal length were used on both transmitting and receiving optics. A scattering angle of receiving optic was set to 70° degrees with slit of 100 µm.

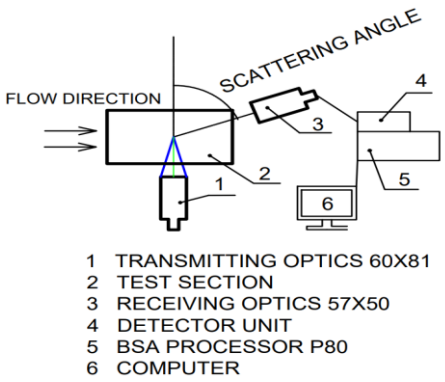

Fig. 2. PDA measurement setup

2.3 High speed visualization

A high-speed camera (FASTCAM SA-Z, Photron, Japan) was used with back illumination by pulsed LED light with 400 ns pulse duration (HPL3-36DD18B, Lightspeed Technologies, USA) to capture the liquid sheet behaviour. 4000 spray images were captured by the camera with a frame rate of 60000 and shutter speed of 1 µm.

2.4 Tested atomizer

A small pressure-swirl atomizer was tested in this study; for dimensions see [7]. The droplets in the range from 0 to 140 µm were created by the breakup of a thin conical liquid sheet.

3 Numerical setup

Description of numerical approaches, boundary condition and computational setup is provided in this chapter.

3.1 Boundary conditions

Boundary conditions were derived from experimental data. Droplet characteristics (velocity, size) were obtained from the PDA measurement. These boundary conditions are outlined in Table 1. Droplets were separated into 4 groups according to their Stokes number. For each droplet group, the velocity magnitude and swirl fraction were determined. The swirl fraction is defined as the ratio of swirl velocity component to the overall liquid velocity inside the spray cone. Since this value is very low, as shown in Table 1, the swirl velocity component can be neglected.

Table 1. Experimental data

Droplet group number [–]	Average group diameter [µm]	Velocity magnitude [m/s]	Swirl fraction [m/s]
1	12.5	18.6	0.006
2	30	20	0.006
3	60	23	0.007
4	110	26	0.008

From instantaneous images (Figure 3), the liquid sheet breakup length was determined to be 7.5 mm with a liquid sheet radius at the breakup length of 4.2 mm. The spray cone angle (SCA) is 60°. All these conditions are determined for the inlet pressure of 0.5 MPa and steady conditions / air flow velocity of 16 m/s.

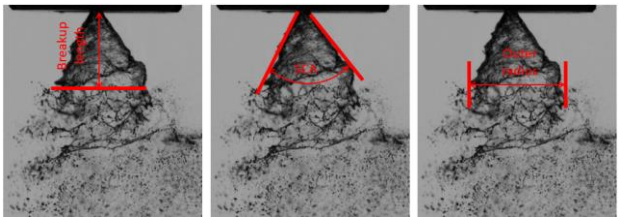

Fig. 3. High speed visualization for air flow of 16 m/s.

3.2 Analytical model

A simple analytical model was developed in MATLAB® software. This model can be used to determine the individual droplet trajectories; this can help in determining the amount of mass involved in the gas scrubbing process, mass trapped by the flow or attached to the walls. The model solves motion equations (Equation 1 and 2) by calculating the drag force and acceleration of droplet, see Equation 3 and 4. and allows for the setting of the initial droplet velocity angle, diameter and cross-flow velocity magnitude and direction. Drag coefficients, C_d, for different ranges of the Reynolds number, Re, incorporated within the model, are described by Equations 5 and 6 [8]. The Runge-Kutta method for solving the differential equation is used within the analytical model.

$$d^2x/dt^2=-(\pi d^2 C_d \rho_g/8m)dx^2/dt \quad (1)$$

$$d^2y/dt^2=g-(\pi d^2 C_d \rho_g/8m)dy^2/dt \quad (2)$$

$$F_d=18\mu C_d Re/[(\rho_l-\rho_g)/\rho_l] \quad (3)$$

$$a=F_d(v-u_l)+g[(\rho_l-\rho_g)/\rho_l] \quad (4)$$

$$Re<1$$

$$C_d=(24/Re) \quad (5)$$

$$1<Re<10^5$$

$$C_d=(24/Re)(1+0.173Re^{0.657})+0.413/(1+16300Re^{-1.09}) \quad (6)$$

3.3 Ansys Setup

3.3.1 Geometry

To simulate the droplet behaviour, the 600 mm long duct with a rectangular cross-section was designed. The geometry is the same as that for the wind tunnel. The injector body was placed 250 mm from the exhaust and inserted 35 mm to the cross-flowing air. The axis origin was set to the nozzle tip. The geometry is illustrated in Figure 4.

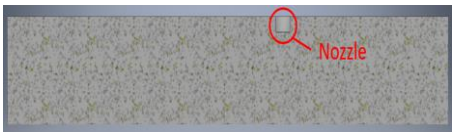

Fig. 4. Geometry of computational domain

3.3.2 Grid independence test

Four differently sized meshes were tested. The node size was 10, 8, 5 and 2 mm with 204268, 304112, 706689 and 7342555 nodes respectively. For the final computation, the mesh with the node size of 5 mm was selected. There was no difference for the nodes of 5 mm and smaller. The droplet trajectories for different mesh sizes and 16 m/s cross-flow velocity is outlined in Figure 5.

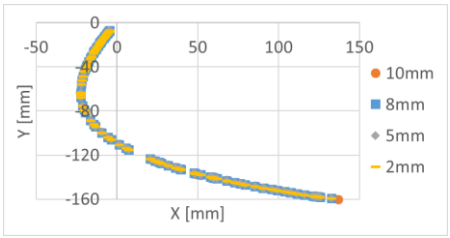

Fig. 5. Comparison of droplet trajectories for differently sized mesh

3.3.3 Mesh

The Ansys mesher was used to generate the structured/unstructured mesh. From the grid independence test, a 5 mm base size was selected. From this setup, the cross-section contains 40×40 nodes. The area of interest for droplet trajectory is in the middle of the model. A standard treatment of wall function was used. The experimentally determined velocity profile is uniform, 12 mm from the walls. The droplet injection was carried out almost 40 mm from the wall.

3.3.4 Physical models

Steady simulation with coupled solver was performed in Ansys fluent. For the turbulence, two-equation k-ε (Realizable) model was selected with scalable wall function. The second order upwind solution for momentum, turbulent kinetic energy, momentum and turbulent dissipation rate was used with presto pressure solution. All models were selected to achieve the simplest case possible.

3.3.5 Boundary conditions

The inlet air velocity was set constant to 8, 16, 32 m/s with turbulent intensity 0.8% at the blue frame in Figure 6. The pressure outlet was set to the opposite side of the model. Other faces were set as walls with no slip boundary and a standard roughness model with roughness constant of 0.5. The droplets that will hit the wall will escape from the simulation domain.

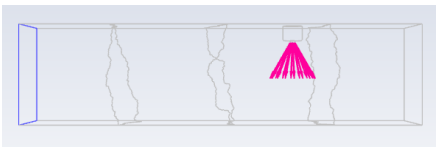

Fig. 6. Boundary conditions

3.3.6 Solution methods

At least 1000 iterations were computed for each case. The continuity, ε and k residuals were lower than 10^{-2}, x, y, and z velocity residuals are lower than 10^{-4} after 1000 iterations.

3.4 Droplet injection

In this section, two methods of droplet injection in ANSYS are described. The Linearized Instability Sheet Atomization (LISA) model and the hollow-cone droplet injection model.

3.4.1 LISA model

The Ansys includes a model for the pressure swirl atomizer simulation (LISA) developed by Schmidt et al. [9]. The LISA model can be divided into two stages, film formation and sheet breakup and atomization (Figure 7)

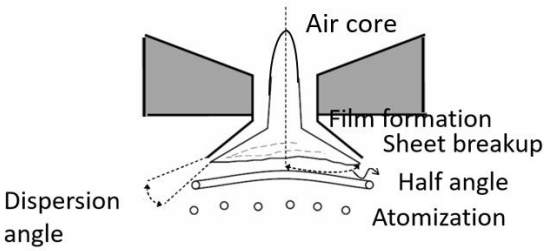

Fig. 7. Schematic process of atomization by LISA model

Sheet constant (S_C) can be derived by equation 5, where L_b is the breakup length, U is the liquid sheet velocity and β is the maximum growth rate. L_b and U can be determined from experimental data. The β can be found in [9] for liquid sheets. It is computed by equation 6, where ρ_L represents the liquid density, γ is the liquid surface tension and ρ is the ratio of air to liquid density.

$$L_b = U \cdot S_C/\beta \quad (5)$$

$$\beta = 0.385\rho^{1.5}(\rho_L U^3/\gamma) \quad (6)$$

The ligament constant (C_L) can be derived from equation 7, where d_L is the ligament diameter at the breakup length and K_S is the wave number corresponding to the maximum growth rate. K_S can be determined by equation 8, where h is the liquid film thickness at the breakup length. h is derived from equation 9, where r_0 is the radius of exit orifice, h_0 is the liquid film thickness at the exit orifice and SCA is the spray cone angle.

$$d_L = 2\pi C_L/K_s \quad (7)$$

$$d_L = \sqrt{8h/K_s} \quad (8)$$

$$h = r_0 h_0/r_0 + L_b \sin(SCA/2) \quad (9)$$

The default values in the fluent are $S_C = 12$, $C_L = 0.5$. From the experimental data the values are S_C=12.7 and C_L = 1.27. There is also a dispersion angle, which defines the amplitude of liquid sheet oscillation. Its value is initially set to 6°.

3.4.2 Droplet hollow-cone injection

For the droplet injection, a cone type injector was used with the boundary conditions outlined in Table 1. Droplets were separated to the groups according to Table 1. The droplet injection was set to the breakup length position on the circle (cone periphery) with outer radius of 4.2 mm. For each droplet group, 720 streams of droplets uniformly distributed on the cone periphery were injected. This corresponds to two droplets streams for every 1° of the cone periphery; the cone angle is 60°.

The spherical drag law is used for droplets injected to the cross-flow. The spherical drag law is expressed by equations 8 and 9. Other ranges of Re can be found in [10].

$$1<Re<10$$

$$C_d = 1.22 + 29.1/Re - 3.8/Re^2 \quad (10)$$

$$1000<Re<5000$$

$$C_d = 0.52 - 1662.5/Re + 5.41/Re^2 \quad (11)$$

4 Results and Discussion

Discrete droplet tracks with hollow cone type injection are illustrated in Figure 8.

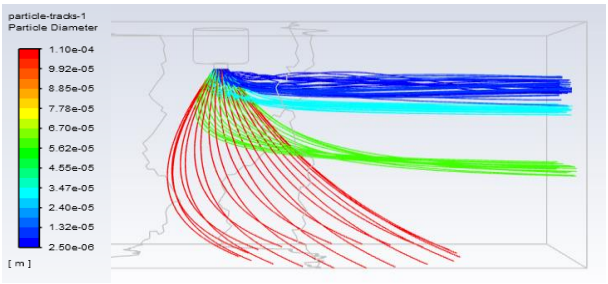

Fig. 8. Discrete droplet tracks for hollow-cone type injector for 8 m/s

The LISA model for the pressure swirl nozzle was employed to compute the track of particles (Figure 9). The droplet size range is from 20 µm to 150 µm. However, the experimental data showed a large fraction of small droplets below 20 µm as these droplets represent as much as 40% of all measured droplets. However, their volume is responsible for only 1.2% of liquid mass. The droplet distribution in LISA model is determined by Rosin-Rammler distribution, which is in agreement with experimental data. Figure 10 shows particle tracks created by analytical model for particle diameter of 110 µm in 16 m/s cross-flow.

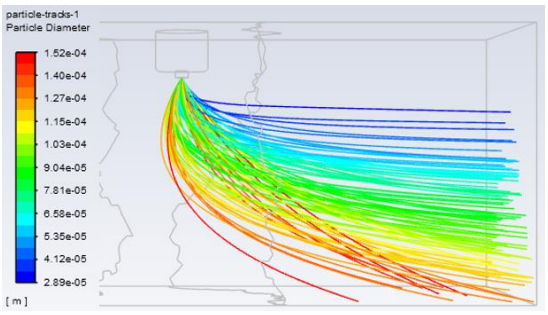

Fig. 9. Particle tracks for LISA for 16 m/s

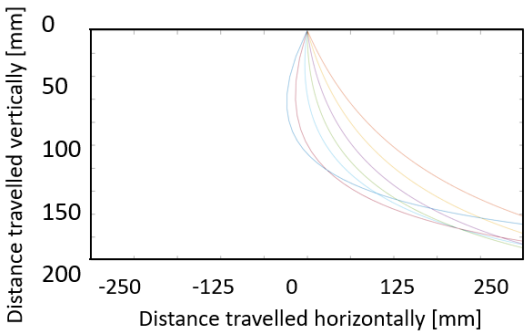

Fig. 10. Particle tracks by analytical code for 16 m/s

4.1 Spray penetration

Spray penetration (penetration length) was determined as the maximum vertical distance that droplets reach after travelling 150 mm downwind from the nozzle. Penetration length for all models and the cross-flow velocity of 16 m/s is illustrated in Figure 11.

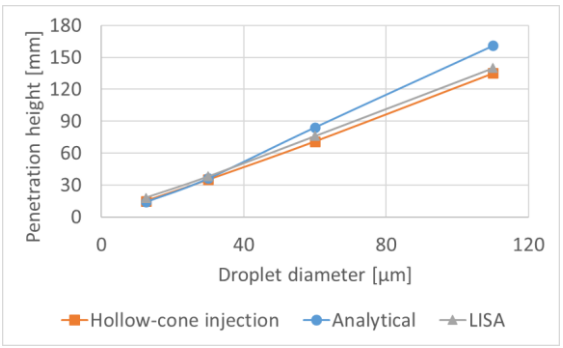

Fig. 11 Penetration length determined by different models for cross-flow velocity of 16 m/s

The penetration height predicted by the hollow-cone injection is almost the same for LISA and analytical models. Some differences occur for large droplets; this can be caused by the oversimplicity of the analytical model.

Figure 12 outlines the penetration of droplets (60 µm) for different *v* and the used numerical approach.

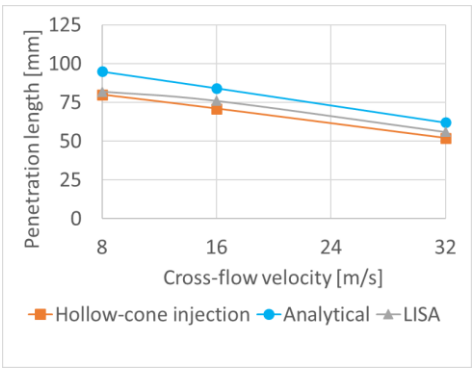

Fig. 12 Comparison of penetration length for different cross-flow velocities and different numerical approaches for 60 µm droplet

4.2 Spray trajectory

The spray trajectory for hollow-cone injection, analytical model and LISA are compared in Figure 13. The trajectory predicted by LISA agrees well with the hollow-cone injection while the trajectory predicted by the analytical model is slightly different; however, with maximum difference below 5%. This small variance can be attributed to only one-way coupling of the analytical model, while both CFD models used a two-way coupling approach.

4.3 Comparison of experimental and numerical results

In Figure 14, the particle trajectories derived by LISA and the analytical model are compared with streamlines derived from experimental PDA data. Streamlines from windward and leeward sides are compared for droplet range of 40 – 80 µm; the LISA model predicts the trajectories really well. analytical models yield higher deviations, which can be caused by oversimplicity of the model with the high-speed image of the spray. It is apparent from the Figure 14 that numerical results and droplet trajectories lie within the high-speed image of the spray. The LISA model is accurate for prediction of droplet trajectories.

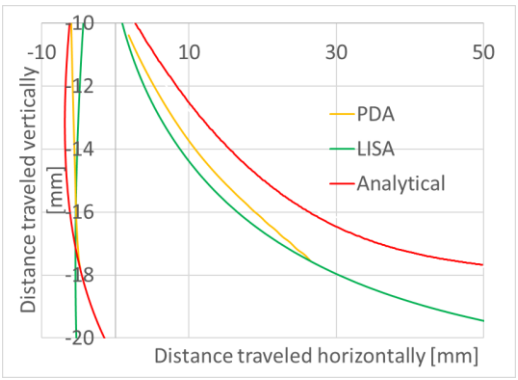

Fig. 13 Comparison of droplet trajectories (40 – 80µm) from leeward and windward sides in cross-flow velocity of 16 m/s for the analytical model, LISA and experimental streamlines created from PDA data

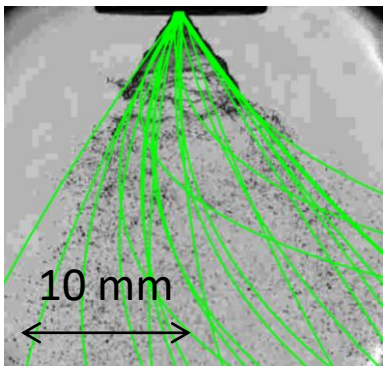

Fig. 14 Comparison of droplet trajectories predicted by LISA and high-speed visualization for 16 m/s

In Figure 15, the droplet diameter predicted by LISA is compared with experimentally obtained PDA data. The results are compared for two axial distances ($Z = 15$ and 20 mm) from the nozzle tip for cross-flow velocity of 16 m/s. As it can be seen from Figure 15, the deviation is slightly larger for $Z = 15$ mm. This can be caused by inaccurate prediction of small droplets by the LISA model. However, for $Z = 20$ mm, the small droplets are usually blown away by the cross-flow and the deviation is much smaller. This is even more apparent for 8 m/s cross-flow velocity as the deviations between the PDA and LISA data were more significant, while for 32 m/s, the results show a good match even for $Z = 15$ mm.

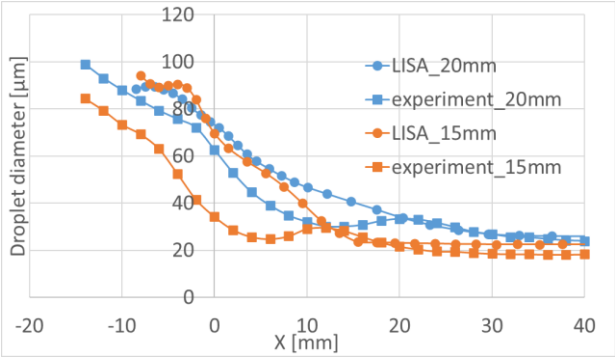

Fig. 15 Comparison of droplet diameter predicted by LISA and obtained by PDA measurement for two axial locations (15 and 20 mm) from the nozzle tip for 16 m/s

5 CONCLUSIONS

The spray behaviour in cross-flow conditions was investigated in this study mainly devoted to the droplet trajectories and behaviour in cross-flow using different approaches. The injection of droplets by the LISA model, a hollow cone injector in Ansys Fluent and a simple analytical model were used to compute the spray/droplet trajectories. Boundary conditions were derived from the experimental results obtained by the PDA and high-speed visualization of the spray in cross-flow. Predicted spray penetration agrees well for all numerical models. Small differences occur in the prediction of penetration of large droplets affected by other physical phenomena, which are not incorporated in the analytical model. With decreasing droplet diameter and increasing cross-flow velocity, the penetration height also decreases. The LISA model predicted the droplet trajectories well.

Droplet trajectories were compared with the experimental data. The LISA method agrees well with the experimental data while the analytical model yields a larger deviation. This can be caused by oversimplicity of this model. A droplet diameter predicted by LISA was compared with experimental results for two planes of 15 and 20 mm from the nozzle tip. The LISA method is not able to predict the behaviour of small droplets (<20 µm) and is more accurate further away from the nozzle where small droplets are drained away.

Nomenclature

a	Acceleration [m·s^{-2}]
C_d	Drag coefficient [–]
d	Droplet diameter [m]
d_L	Ligament diameter at the breakup length [m]
Fd	Drag force [N]
g	Gravitational acceleration [m·s^{-2}]
h	Liquid film thickness at the breakup length [m]
h_0	Liquid film thickness at the exit orifice [m]
K_S	Wave number corresponding to the maximum growth rate [–]
L_b	Breakup length [m]
m	Droplet mass [kg]
r_0	Radius of exit orifice [m]
Re	Reynolds number [–]
S_C	Sheet constant [–]
SCA	Spray cone angle [°]
Tu	Turbulent intensity [%]
U	Liquid sheet velocity [m·s^{-1}]
u_l	Droplet velocity [m·s^{-1}]
V	Cross-flow velocity [m·s^{-1}]
x	Distance in x direction [mm]
y	Distance in y direction [mm]
Z	Axial location from the nozzle [mm]
Greek characters	
β	Maximum growth rate [–]
γ	Liquid surface tension [N·m^{-1}]
ρ	Ratio of air to liquid density [kg·m^{-3}]
ρg	Density of gas [kg·m^{-3}]
ρ_l	Density of liquid [kg·m^{-3}]

Acknowledgment

The authors acknowledge the financial support from the project no. LTAIN19044 program INTER–EXCELLENCE (INTER–ACTION), project Quality Internal Grants of BUT (KInG BUT), Reg. No. CZ.02.2.69 / 0.0 / 0.0 / 19_073 / 0016948, which is financed from the OP RDE and from No. FSI-S-20-6295 founded by Faculty of Mechanical Engineering, Brno University of Technology.

References

1 J. H. Kim, R. D. Reitz, and S. W. Park, Proceedings of the Institution of Mechanical Engineers, Part D: Journal of Automobile Engineering **224** (8), 1113 (2010).
2 S. K. Amedorme and J. Apodi, AIP Conference Proceedings **2016** (1), 020026 (2018).
3 S. Deshpande, Atomization and Sprays **21** (2011).
4 H. Zhang, H. Zhang, and B. Bai, Heat Transfer Engineering, 1 (2021).
5 H. Sun, B. Bai, and H. Zhang, Heat Transfer Engineering **35** (6-8), 664 (2014).
6 S. Dikshit, D. Kulshreshtha, and S. Channiwala, *Numerical simulation of Pressure Swirl Atomizer for Small Scale Gas Turbine Combustion Chamber*. (2017).
7 M. Maly, J. Jedelsky, J. Slama, L. Janackova, M. Sapik, G. Wigley, and M. Jicha, International Journal of Heat and Mass Transfer **123**, 805 (2018).
8 R. L. C. Flemmer and C. L. Banks, Powder Technology **48** (3), 217 (1986); R. Turton and O. Levenspiel, Powder Technology **47** (1), 83 (1986).
9 D. Schmidt, I. Nouar, P. Senecal, J. Hoffman, C. Rutland, J. Martin, and R. Reitz, *Pressure-Swirl Atomization in the Near Field*. (1999).
10 S. A. Morsi and A. J. Alexander, Journal of Fluid Mechanics **55** (2), 193 (1972).